

A new approach to NO₂ Gas sensing based on Pulsed UV light and FFT analysis using MOX sensors

Ernesto González, Eduard Llobet, *Senior Member, IEEE*, Alfonso Romero, Xavier Vilanova

Abstract—Metal Oxide Semiconductor gas sensors have been recently temperature modulated, and UV light activated to improve their sensitivity and selectivity. In this work, we present the first known development of calibration models, using pulsed UV light modulation for WO₃ based gas sensing. Partial Least Squares Regression (PLSR) and Principal Component Regression (PCR) methods have been developed using components from the FFT analysis of the DC resistance signal of the sensor. The use of pulsed UV light, combined with low-temperature activation allowed a significant reduction in power consumption as compared to the high operating temperature traditionally used with Metal Oxide non-MEMs-based sensors. The methodology proposed in this study allows diminishing the time necessary to determine the concentration, with the reduction of the pulsed UV light period, and the number of pulses used for this purpose, in respect to the use of resistance rate analysis, as proposed by other authors. The FFT analysis made before performing the linear regression methods allows the diminution of the prediction error from the models, as compared to the rate analysis. These advantages present a progress over the analysis of the rates from the resistance signal, recently presented by other authors. The correct performance of the presented procedure, working with NO₂ concentrations under harmful exposure limits, opens the opportunity of using this methodology in real air quality applications.

Index Terms— Calibration model, gas sensing, pulsed UV light.

I. INTRODUCTION

DURING the past decade, the air quality monitoring, both, in indoor and outdoor environment has captured the interest of many researchers, due to its direct influence in human health [1]–[3]. The widespread applications of metal oxide semiconductors for gas sensing purposes have led them to be some of the most used materials in the detection of environmental pollutants [4], [5].

Metal Oxide Semiconductor (MOX) gas sensors have been widely studied by decades due to their high sensibility and reversible absorption and desorption interactions between these materials and target gases [6]–[8]. The operating principle of MOX sensors is based on redox reactions occurring between

the target gas and the metal oxide surface of the active layer of the sensor. During the redox reaction, oxygen species adsorbed on the metal oxide react with molecules of the target gas producing an electronic interchange, which is measured as a resistance change of the sensor [4].

For many years, MOX sensors have been typically used by applying operating temperatures in the range 100–500 °C to improve their response and sensitivity, which implies a considerable power consumption to heat the sensors [9]–[11]. However, a few years ago, the UV-irradiation of MOX sensors has been studied as an alternative to the more traditional thermally activated gas sensing [12]–[14]. UV light provokes the generation of electron/hole pairs, induced by the photoconductivity effect, which increases the density of charge carriers through the semiconducting layer, improving the absorption/desorption mechanism [15], [16]. The effect of constant UV light has been normally used for improving the sensor response at low or even at room temperature operation [17]–[20]. In addition, UV irradiation during the recovery phase only has been employed for decreasing the recovery time via increasing the desorption rate [21], [22]. Nevertheless, recently, a new pulsed UV light method has been developed [23], [24], and used in a portable gas sensing system [25], working at low or room temperature. This method allows determining the gas concentration by analyzing the resistance change, a ripple caused by the effect of the UV light being switched ON and OFF [24].

On the other hand, several researchers have used mathematical data analysis and statistical methods to quantify the concentration of a target gas and determine the Limit of Detection (LOD) of MOX sensors [26]–[28]. The use of Principal Component Analysis (PCA), and the development of calibration models using Principal Component Regression (PCR) and Partial Least Square Regression (PLSR) have permitted to determine the target gas concentration in gas sensing applications (e.g., CO, NO₂, volatile compounds, among others) [26]–[30]. While most of these studies have implemented the data analysis methods using the DC signal of

This paragraph of the first footnote will contain the date on which you submitted your paper for review. This work has been funded in part by MINECO under grant No. TEC2015-71663-R, by the European Commission via the European Regional Development Fund (ERDF) and AGAUR under grant 2017SGR 418. E.G. is supported by AGAUR under pre-doctoral grant 2018 FL_B 00496. E.L. is supported by ICREA under the 2018 Edition of the ICREA Academia Award.

Ernesto González, Eduard Llobet, Alfonso Romero and Xavier Vilanova are with the MINOS research group, Department of Electronic, Electric and Automatic Engineering, School of Engineering, University Rovira i Virgili, Tarragona 43007, Spain. e-mail: ernesto.gonzalez@urv.cat; eduard.llobet@urv.cat; alfonsojose.romero@urv.cat; xavier.vilanova@urv.cat.

the sensors working under temperature modulation [27], [29], [30], some researchers have reported the use of components from the Fast Fourier Transform (FFT) analysis of the resistance transients as input data for these analysis methods. This methodology has become an excellent tool for determining gas concentration and discriminating different gases [31], [32]. This work presents the development of calibration models of a tungsten trioxide (WO_3) based pulsed UV light modulated gas sensor, based on the above-mentioned research background. Combined low temperature and pulsed UV light configuration are used for measuring NO_2 at ppb level. The FFT components from the analysis of the resistance signal of the sensors are used as input of the PCR and PLSR methods. The use of the FFT components instead of the resistance rate obtained from the pulsed UV light modulation represents an improvement of the methodology developed by Gonzalez. et al [24]. The results, obtained from models developed using FFT components, are compared with those obtained from the resistance rates (used by Gonzalez. et al).

II. EXPERIMENTAL

A. Sensor Fabrication

The sensors used in this work were made following a well-known technique based on aerosol assisted chemical vapor deposition (AACVD), widely used in previous works to synthesize tungsten trioxide (WO_3) nanoneedles or nanowires [33]–[36]. We synthesized WO_3 nanoneedles on a commercial alumina substrate, containing platinum interdigitated electrodes with a 300 μm gap on the top side and 8 Ω heater on the bottom side, from Ceram Tech GmbH. 50 mg of tungsten hexacarbonyl ($\text{W}(\text{CO})_6$) were dissolved in a mixture of 15 ml of acetone and 5 ml of methanol. Vapor from the dissolution was generated by means of an ultrasonic humidifier, and nitrogen was used as carrier gas with a flow of 200 sccm. With this approach, about 45 min were necessary to transport all the dissolution inside the deposition chamber and complete the nanoneedle growth. The temperature of the deposition chamber was kept at 400 $^\circ\text{C}$ during the deposition time and then naturally cooled to room temperature. Once the nanoneedles were grown, an annealing process was made at 500 $^\circ\text{C}$ during 2 h in a Carbolite CWF 1200 muffle furnace, in order to fully oxidize the WO_3 and remove the residual carbon from the precursor.

B. Measuring system description

Measurements were made inside a Teflon chamber with an inner volume of 21.18 cm^3 , and capacity for measuring 4 sensors at the same time. The chamber has 2 holes at the top, through which the UV light LEDs are inserted. Inside the chamber, sensors are totally isolated from the ambient light. Sensor resistance was measured and recorded at a frequency of 1 Hz by using a Keysight 34972A LXI Data Acquisition/Switch Unit controlled with BenchLink Data Logger 3 from Agilent Technologies.

Different gas concentrations were established by mean of a mass flow control system, using EL-FLOW mass flows from Bronkhorst, controlled using Flow View and Flow Plot

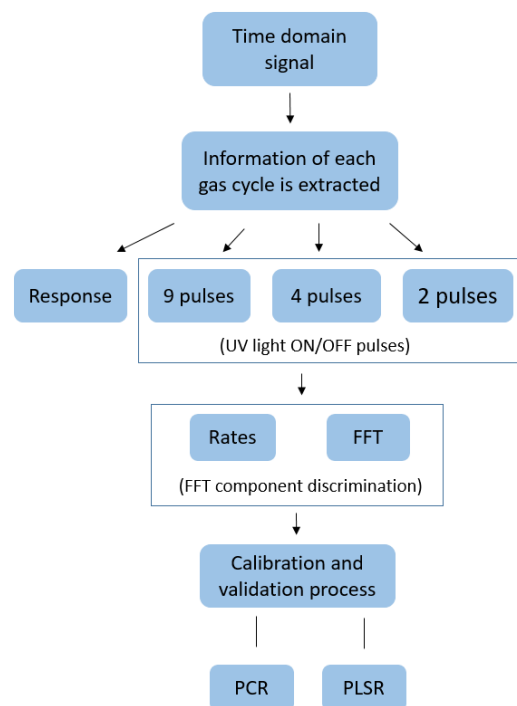


Fig. 1. Flow diagram of the data analysis process.

software from Bronkhorst. This system was used to mix the gases coming from a bottle of dry, zero-grade air, and the one coming from a bottle containing a dilution of 1 ppm of NO_2 , balanced in dry air in the adequate proportion to achieve the desired concentration, keeping the total flow across the sensors chamber constant at 100 ml/min.

Sensors were exposed, in a first stage, to NO_2 concentrations in the range of hundreds of ppbs to validate the procedure and tens of ppbs later to check the viability of the system to detect NO_2 below the daily limit of exposure established in the EU ambient air quality directives [38]. During the first stage, a gas exposure cycle consisted of a set of measurements in the 200 to 900 ppb concentration range (with an increase of 100 ppb between consecutive measurements). The second set of measurements were performed using cycles of 37.5, 75, and 150 ppb. All of the measurements were made using 15 min of NO_2 exposure and then 1 h of baseline recovery under dry air. An extra recovery time of 1 h was set between any two consecutive cycles.

In order to carry out this study, we used a combined configuration of UV pulsed light and low-temperature heating. Operating temperature of the sensors was set at 50 $^\circ\text{C}$ using the heater placed on the backside of the substrate. The UV LEDs used emit at a wavelength of 325 nm [39], which correspond to a photon energy of 3.82 eV. The UV light was switched ON and OFF, using periods of 60 and 30 s, in order to compare results when the period of UV irradiation changes. For both of the periods used, the duty cycle applied was 50%.

C. Data Analysis Process Description

In order to generate a model which allows us to identify the concentration of studied gas, mathematical and computational tools were used, such as, FFT, PCR, and PLSR. All data analysis was carried out by using MATLAB R2017b. Fig. 1

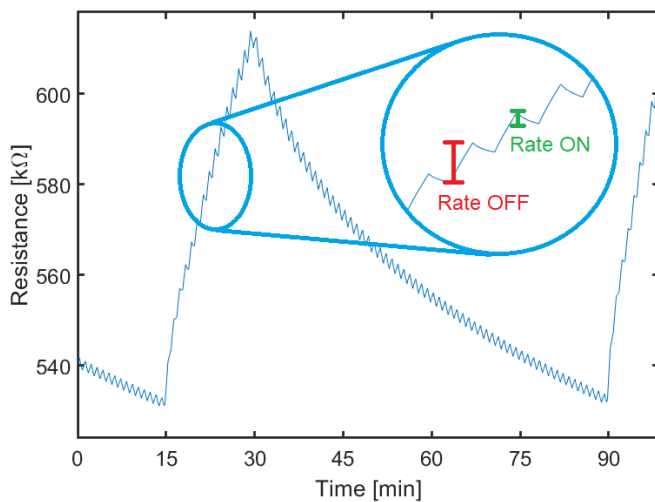


Fig. 2. Sensor signal rates ON (when the UV light is turned ON) and OFF, (when the UV light is turned OFF).

shows the flow diagram of the data analysis process.

The purpose of this study is to find a faster way to identify and quantify gas concentrations in comparison to standard methods, which need the total saturation of the sensor response and the full recovery of its baseline resistance [35]–[37]. Moreover, we look for the reduction of the time needed to quantify a concentration proposed by other authors, using the same pulsed UV light mechanism [24]. On the other hand, this approach reduces the power consumption because of the decrease of the operating temperature of the sensor, which is generally set in the range 100–500 °C when metal oxide (MOX) gas sensors are used [12]. We propose to apply a frequency domain analysis to the sensor signal, which, due to the UV modulation, shows a ripple superimposed to the electrical resistance change due to gas exposure. During the semi-period in which UV light is off, just the reaction of a target gas with the sensor surface material influences sensor response, while in the semi-period in which UV light is on, UV light influences sensor response too. Tungsten trioxide is an n-type MOX, which has a bandgap of about 2.7 eV [40]. The photon energy of the UV LEDs we used is 3.82 eV, as we mentioned above, which is higher than the energy gap of the material. When UV light is on, this causes an interband electronic transition elevation, causing thus an increase in the electrical conductance.

In order to carry out the study of this new method, we have generated some data sets, using information about measurements made over 7 months.

1) Models employing the rates of resistance change

First of all, the time domain sensor signal is obtained. From this signal we obtain sensor response for each gas cycle (R_g/R_a) and rates (taken as the resistance change between the moment when the UV light is turned on, and the moment in which it is turned off, for rate ON, and vice versa for the rate OFF). This is shown in Fig. 2 (following the procedure described by Gonzalez. O et al [24]). These resistance changes appear in this work as rate ON and rate OFF. In our case, the models

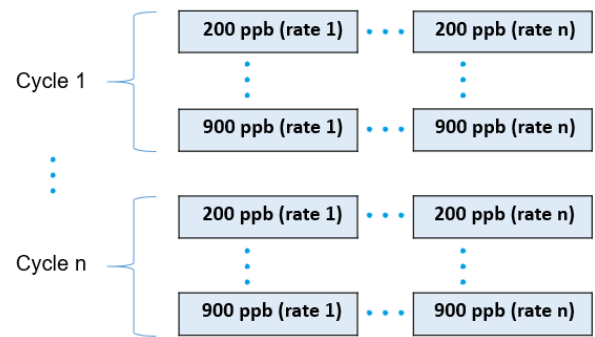


Fig. 3. Data set used to construct the training data in the case of rates analysis.

developed used exclusively the OFF rates, since in this semi-period, only the reaction of the target gas with the active layer influences sensor response. Since the gas exposition time set was 15 minutes, using a UV light ON/OFF period of 60 s we would have 15 pulses or UV light periods, and ON/OFF rates. As Fig. 2 shows, the sensors present a different behavior in the firsts pulses of each gas exposure cycle. This is caused by the time needed to establish a homogeneous gas concentration inside the chamber after changing from exposure to synthetic air to a fixed gas concentration. This is why in the modeling process, the first six pulses are not used in the analysis, which allowed us to use a maximum amount of 9 pulses. Results from models obtained using a different number of pulses or UV light periods are compared, to analyze the influence of this parameter on the calibration process, while reducing the time needed to determine a given gas concentration. With this purpose, we have developed up to three models using different number of UV light periods. These three models employed sets of 9 periods (from the 7th to the 15th period), 4 periods (from 7th to 10th) and 2 periods (7th and 8th), respectively. Fig. 3 shows the composition of one of the data sets we used as training data. We built PCR and PLSR models using training matrices considering different number of pulses (2, 4 and 9).

In order to compare the results of those models obtained employing different number of pulses, we took into account three parameters: standard deviation of each estimated concentration by the model as a percent of the real concentration, the root mean square error (RMSE) of the model, and the R-squared (R^2) value. On the other hand, we compared these parameters for PCR and PLSR models to find the best modeling method. Both, PCR and PLSR methods were developed using only the first two principal components or latent variables, respectively, because these components explained over 99% of the data variance in all cases. The improvement in concentration prediction by adding further factors to the models was lower than 1%.

As a new approach, we considered applying an FFT to the time domain signal, using this information to generate the models. Therefore, we compared the performance of both approaches, by using the parameters mentioned above.

2) Models employing the FFT

After taking vectors from the time domain signal with 2, 4 and 9 UV light periods from each gas concentration response as

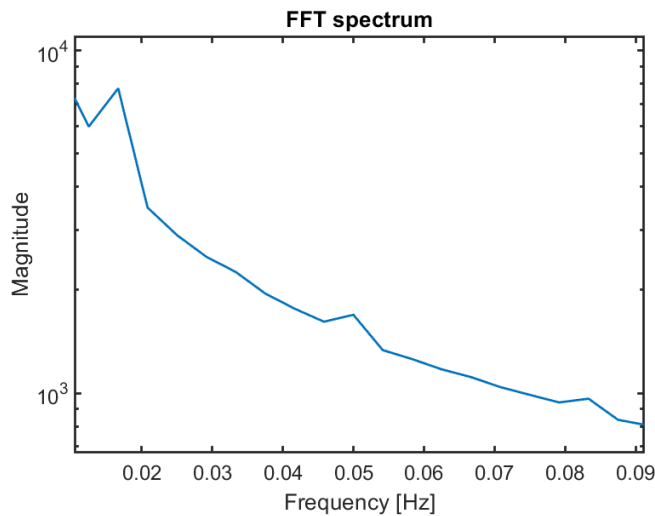


Fig. 4. FFT spectrum of sensor signal taking pulses from 7 to 10 after starting the exposition to gas. The spectrum shows frequency components (peaks) belonging to the UV light ON/OFF period and its two first even order harmonics (from left to right).

in the previous case, we computed an FFT of each one in order to perform a frequency domain analysis. Since the sampling rate used over all of the measurements performed was 1 Hz, the size of the vectors used to develop the FFT analysis depends on the number of pulses used with this purpose, e.g., with a UV light period of 60 s, using 9 pulses to carry out the analysis, vectors contain 540 values. Although the number of FFT components obtained from the FFT analysis is half of the number values used to develop it, we did not use all of them. FFT vectors were manipulated in order to remove components that did not provide relevant information. For this purpose, we analyzed what other components, apart from the direct component (0 Hz), appeared in spectra. As Fig. 4 shows, we found that a component corresponding to UV light switching period (for 60 s period the corresponding frequency is 0.01667 Hz) and its even order harmonics appeared in the FFT spectrum. Therefore, we generated a new vector, which contained just values corresponding to the frequencies of interest (ON/OFF frequency and a set of its even order harmonics) in order to reduce the amount of data used in the modeling process and, in this way, avoid using low-intensity frequency components that may be prone to be affected by noise. Finally, we used just the UV light switching frequency and its 2 first even order harmonics as using a higher amount of FFT components did not improve the prediction error or the standard deviation of the model. We constructed a training matrix containing concatenated vectors for each concentration. In this matrix, rows are different concentrations and columns are frequency components of interest. The data sets of the training data were similar to those which appears in Fig. 3, but, instead of rates, the FFT components were used.

III. RESULTS AND DISCUSSION

The use of combined pulsed UV light and low-temperature heating as the activating mechanism, instead of the traditional high operating temperature, allowed a significant reduction in

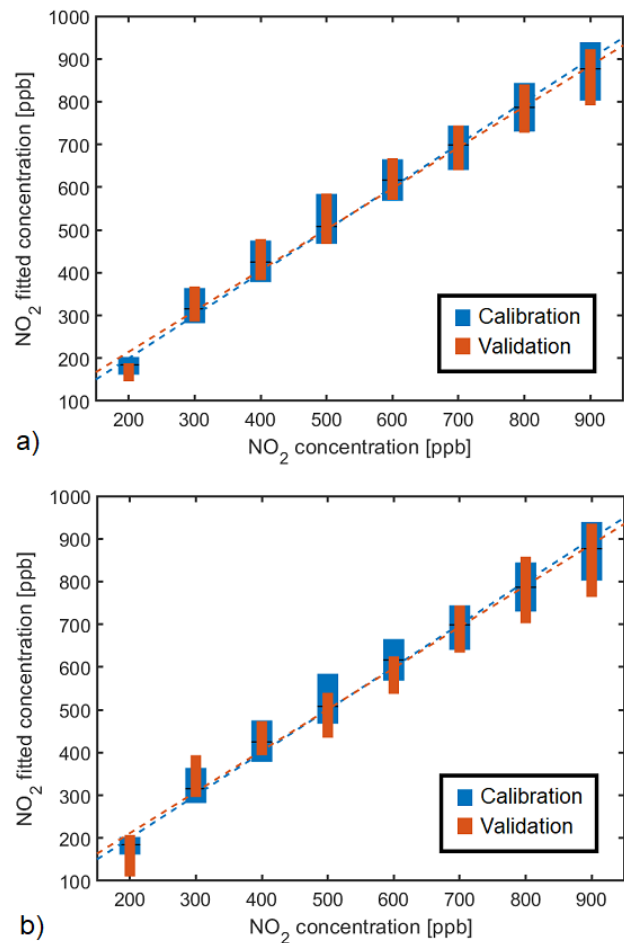


Fig. 5. PLSR calibration model and cross-validation from 9 pulses a) rates OFF and b) FFT components. Blue boxes represent the dispersion of the calibration for each concentration and orange boxes represent the validation dispersion. Black lines are the calibration mean value for each concentration. The linear calibration fit and the linear validation fit are presented in blue and orange dashed lines, respectively.

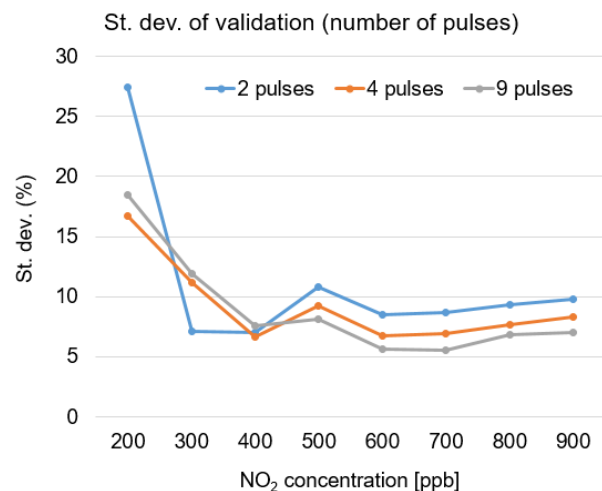


Fig. 6. The standard deviation of the PLSR model's validation made from the rates OFF, depending on the number of pulses, working with a UV light period of 60 s.

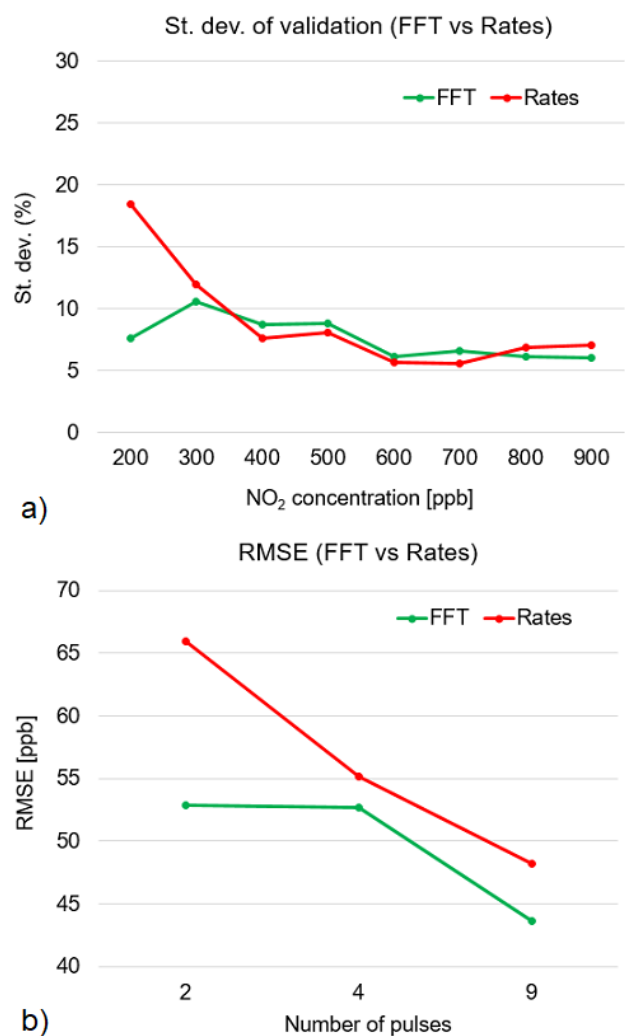


Fig. 7. Comparison between PLSR models validation obtained from rates and FFT from 4 pulses, with a UV light ON/OFF period of 60 s, depending on a) the standard deviation as percent of the real concentration and b) the RMSE of them.

power consumption. In this case, we used an average power of 136 mW to heat up the sensor and turn the UV LEDs on, of which just 25 mW are used to power de LEDs on, while using an operating temperature of 250 °C, power consumption was 1.6 W. This means we saved more than 90% of the power needed to activate the sensing layer, which is quite significant when working with this kind of sensors, although it is less relevant in the case of MEMs based MOX sensors.

We used cross validation to estimate the accuracy of the different models to predict NO₂ concentrations. Thus, we applied a leave-one-out strategy. For the concentrations range 200-900 ppb, and 300-900 ppb, we used 8 and 4 iterations, respectively, leaving all the data about one concentration out of the training set, and using it as validation set each time. In the case of the concentration range of 37.5-150 ppb, the above mentioned distribution of the training and validation sets did not allow the proper prediction of NO₂ concentrations. This, due to in this range there were just three different concentrations. In this way, we used the leave-one-out strategy generating the training set with five cycles of three concentrations and leaving one cycle as validation set. We made 6 iterations rotating the

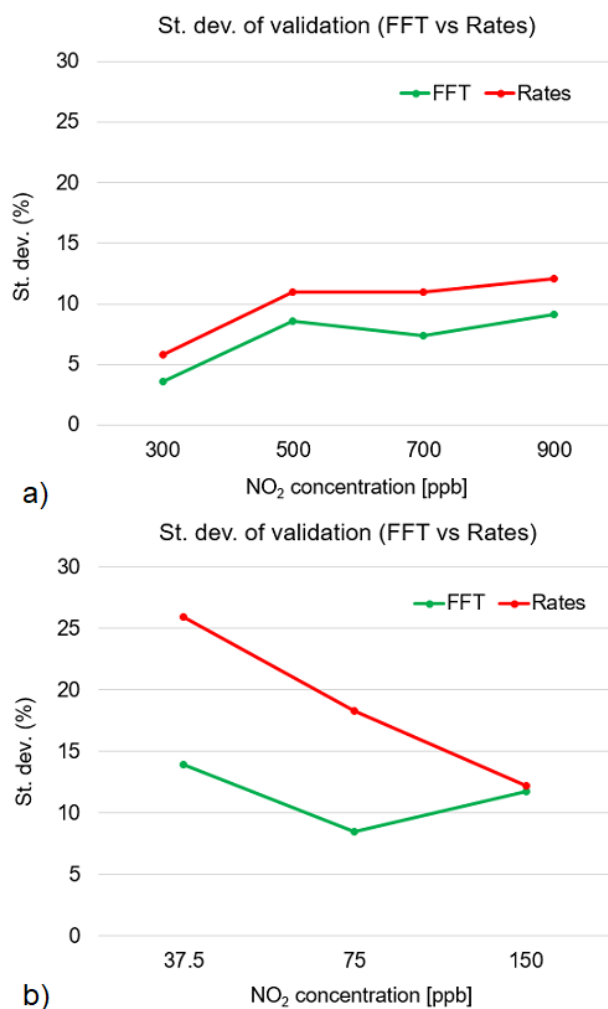


Fig. 8. Comparison between the standard deviation of PLSR models validation obtained from rates and FFT from 4 pulses, with a UV light ON/OFF period of 30 s, a) in the range 300- 900 ppb and b) in the range 37.5-150 ppb.

TABLE I
 MODELS´ RMSE AND R-SQUARED VALUES FROM 4 PULSES ANALYSIS FOR VALIDATION PROCESS

Model	Period [s]	Range [ppb]	RMSE [ppb]	R ²
PCR (Rates)	60	200-900	55.2	0.9392
PCR (FFT)	60	200-900	52.7	0.9454
PLSR (Rates)	60	200-900	55.2	0.9394
PLSR (FFT)	60	200-900	55.6	0.9454
PCR (Rates)	30	300-900	73.5	0.8592
PCR (FFT)	30	300-900	71.0	0.9035
PLSR (Rates)	30	300-900	75.7	0.8468
PLSR (FFT)	30	300-900	71.1	0.9033
PCR (Rates)	30	37.5-150	23.6	0.6671
PCR (FFT)	30	37.5-150	10.5	0.94.91
PLSR (Rates)	30	37.5-150	21.8	0.7285
PLSR (FFT)	30	37.5-150	10.5	0.9491

validation set to evaluate the performance of whole data set.

The results obtained from models developed using the OFF rates, studied by Gonzalez. et al [24] were compared with those from models created using the FFT components. Fig. 5 depicts the PLSR calibration model and validation obtained for a) FFT components and b) OFF rates using 9 pulses, with a UV light period of 60 s. We can observe how models obtained from FFT components present more accuracy in prediction performance than models obtained from OFF rates.

The use of PLSR and PCR do not result in significant differences in standard deviation, and RMSE and R^2 values.

In Fig. 6 we can observe how changes in the number of pulses used to build the training sets result in little changes in the uncertainty associated to the prediction of concentrations. The standard deviation of the model decreases when the number of pulses used in training matrix increases. Namely, the standard deviation of the predictions remains under 10 % for most of the concentrations estimated, regardless the number of pulses used. The estimation of low concentrations presents higher standard deviations, which can be attributed to higher errors from the mass flow controller systems at low valve openings.

As Fig. 7a shows, the calibration model obtained from FFT components has a better behavior at 200 ppb than the model obtained from the rates OFF. The differences in standard deviation between models from FFT and rates can be explained by the fact that with the FFT we obtain more information from the signal than with just the resistance rates. The RMSE values from the PLSR FFT model, shown in Fig. 7b, are lower than those from the rates model for all concentrations. A maximum difference of 13 ppb was found in the case of models obtained using 2 signal pulses. Although the R^2 values from the models have close values for all cases, models from FFT components always present higher values.

Results obtained for PCR and PLSR models, using both rates and FFTs, for a UV light ON/OFF period of 60 s, do not present notable differences. Nevertheless, when reducing the number of pulses analyzed, with the purpose of reducing the time to determine a concentration in a real application, the best results are obtained for models created using FFT components. Table I shows RMSE and R^2 values for models obtained analyzing 4 UV light periods of the signal.

Once we had obtained the models using an ON/OFF period of 60 s, we prepared some additional data sets using a period of 30 s to test the feasibility of the procedure developed, with the reduction of the identification time. This means, in turn, a reduction in the time necessary to determine a target gas concentration. In this part of the study, we applied the modeling process using the previously studied concentrations, and then, using a concentrations range of 37.5-150 ppb. It allowed us to apply this method to determine concentrations under the exposure limit established by the European Environment Agency [38].

Working with a UV light period of 30 s, results obtained from calibration models made from rates and from FFT components, have significant differences. Fig. 8 shows the standard deviation for PLSR models obtained working in a concentration range of 200-900 ppb (8a) and 37.5-150 ppb (8b). For both

concentration ranges, the standard deviation for almost all concentrations is lower in the case of models made from FFT components, even with a difference higher than 10% for 37.5 ppb. Results presented in Fig. 8 are supported by those shown in Table I. We can observe how models from FFT components have lower RMSE and higher R^2 values than those obtained from rates, for both PCR and PLSR analysis and both concentration ranges. These results support and justify the development of this new method, combining FFT analysis with linear regression methods. When reducing both the amount of UV light pulses analyzed and the UV light period, looking for decreasing the time required to determine the gas concentration, we obtained the best results for models developed from FFT components.

The response time of the WO_3 gas sensor to NO_2 concentrations in the range between a few ppm and hundreds of ppb is about 10 min [41], [42]. With a pulsed UV light period of 30 s, and using 4 pulses to develop the methodology presented, we determine the NO_2 concentration in just 2 min. This means we save 80% of the time needed to determine the target gas concentration, while the power consumption is reduced about a 90% as compared with high temperature heated methodologies.

IV. CONCLUSION

We have proposed the combined use of FFT analysis and linear regression methods to obtain calibration models that allow us to determine NO_2 concentrations using a WO_3 based sensor. The combined pulsed UV light and low-temperature heating configuration used as activating mechanism represents a reduction in power consumption of about 90% as compared to the traditional heating mechanism at 250 °C. This approach also allows a reduction of the response time, since the concentration can be determined without requiring the sensor resistance to reach the steady state value. The calibration models obtained from the FFT analysis proposed in this study lead to better results than the ones elaborated using the rates OFF, approach presented by other researchers, when the pulsed UV light period is diminished in order to further reduce the required time to determine the gas concentration. Moreover, the best results are also obtained for models based on the FFT analysis when working with low concentrations, under the exposure limits defined for nitrogen dioxide.

The methodology presented in this work will be used with different active layer materials and target gases. A configuration of an array of sensors will be implemented to make cross sensitivity tests using this procedure.

REFERENCES

- [1] R. D. Stephens and S. H. Cadle, "Remote sensing measurements of carbon monoxide emissions from on-road vehicles," *J. Air Waste Manag. Assoc.*, vol. 41, no. 1, pp. 39–46, 1991.
- [2] X.-Z. Chen and J. Yu, "Development of Metal Oxide Gas Sensors for Environmental Security Monitoring: An Overview," Springer, Cham, 2015, pp. 215–227.
- [3] A. Szczurek and M. Maciejewska, "Gas sensing method applicable

- to real conditions," *Meas. Sci. Technol.*, vol. 24, no. 4, 2013.
- [4] X. Liu *et al.*, "A Survey on Gas Sensing Technology," *Sensors*, vol. 12, no. 7, pp. 9635–9665, Jul. 2012.
- [5] Z. Wang *et al.*, "Study on highly selective sensing behavior of ppb-level oxidizing gas sensors based on Zn₂SnO₄ nanoparticles immobilized on reduced graphene oxide under humidity conditions," *Sensors Actuators, B Chem.*, vol. 285, no. December 2018, pp. 590–600, 2019.
- [6] Z. Fan and J. G. Lu, "Metal Oxide Nanowires: Fundamentals and Sensor Applications," in *Metal Oxide Nanomaterials for Chemical Sensors*, New York, NY: Springer New York, 2013, pp. 287–319.
- [7] K. Yamazoe, N., Shimano, "Overview of gas sensor technology," in *Science and Technology of Chemiresistor Gas Sensors*, Nova Science Publishers, Inc., 2007, pp. 1–31.
- [8] E. E. Bassey, P. Sallis, and K. Prasad, "Sensitivity Variation of Nanomaterials at Different Operating Temperature Conditions," Springer, Cham, 2017, pp. 447–452.
- [9] D. Zappa, V. Galstyan, N. Kaur, H. M. M. Munasinghe Arachchige, O. Sisman, and E. Comini, "Metal oxide -based heterostructures for gas sensors'- A review," *Anal. Chim. Acta*, vol. 1039, pp. 1–23, 2018.
- [10] S. Vallejos *et al.*, "Au nanoparticle-functionalised WO₃ nanoneedles and their application in high sensitivity gas sensor devices," *Chem. Commun.*, vol. 47, no. 1, pp. 565–567, 2011.
- [11] S. Vallejos *et al.*, "Single-step deposition of au- and pt-nanoparticle-functionalized tungsten oxide nanoneedles synthesized via aerosol-assisted CVD, and used for fabrication of selective gas microsensor arrays," *Adv. Funct. Mater.*, vol. 23, no. 10, pp. 1313–1322, 2013.
- [12] E. Comini, G. Faglia, and G. Sberveglieri, "UV light activation of tin oxide thin films for NO₂ sensing at low temperatures," *Sensors Actuators, B Chem.*, vol. 78, no. 1–3, pp. 73–77, 2001.
- [13] B. P. J. de Lacy Costello, R. J. Ewen, N. M. Ratcliffe, and M. Richards, "Highly sensitive room temperature sensors based on the UV-LED activation of zinc oxide nanoparticles," *Sensors Actuators, B Chem.*, vol. 134, no. 2, pp. 945–952, 2008.
- [14] J. D. Prades *et al.*, "Equivalence between thermal and room temperature UV light-modulated responses of gas sensors based on individual SnO₂nanowires," *Sensors Actuators, B Chem.*, vol. 140, no. 2, pp. 337–341, 2009.
- [15] O. Lupan, V. Postica, J. Grötrrup, A. K. Mishra, N. H. de Leeuw, and R. Adelung, "Enhanced UV and ethanol vapour sensing of a single 3-D ZnO tetrapod alloyed with Fe₂O₃nanoparticles," *Sensors Actuators, B Chem.*, vol. 245, pp. 448–461, 2017.
- [16] F. Taghipour, "UV-LED Photo-activated Chemical Gas Sensors: A Review AU - Espid, Ehsan," *Crit. Rev. Solid State Mater. Sci.*, vol. 42, no. 5, pp. 416–432, Sep. 2017.
- [17] N. D. Chinh, C. Kim, and D. Kim, "UV-light-activated H₂S gas sensing by a TiO₂ nanoparticulate thin film at room temperature," *J. Alloys Compd.*, vol. 778, pp. 247–255, Mar. 2019.
- [18] S. Park, T. Hong, J. Jung, and C. Lee, "Room temperature hydrogen sensing of multiple networked ZnO/WO₃ core-shell nanowire sensors under UV illumination," *Curr. Appl. Phys.*, vol. 14, no. 9, pp. 1171–1175, 2014.
- [19] A. Ilin *et al.*, "UV effect on NO₂ sensing properties of nanocrystalline In₂O₃," *Sensors Actuators, B Chem.*, vol. 231, no. 2, pp. 491–496, 2016.
- [20] Y. Li *et al.*, "Synthesis of novel porous ZnO octahedrons and their improved UV-light activated formaldehyde-sensing performance by Au decoration," *Phys. E Low-dimensional Syst. Nanostructures*, vol. 106, pp. 40–44, Feb. 2019.
- [21] O. Lupan *et al.*, "Selective hydrogen gas nanosensor using individual ZnO nanowire with fast response at room temperature," *Sensors Actuators, B Chem.*, vol. 144, no. 1, pp. 56–66, 2010.
- [22] S. Trocino *et al.*, "Gas sensing properties under UV radiation of In₂O₃ nanostructures processed by electrospinning," *Mater. Chem. Phys.*, vol. 147, no. 1–2, pp. 35–41, 2014.
- [23] O. Gonzalez, S. Roso, R. Calavia, X. Vilanova, and E. Llobet, "NO₂ sensing properties of thermally or UV activated In₂O₃nanooctahedra," *Procedia Eng.*, vol. 120, no. 2, pp. 773–776, 2015.
- [24] O. Gonzalez, T. Welaregay, E. Llobet, and X. Vilanova, "Pulsed UV Light Activated Gas Sensing in Tungsten Oxide Nanowires," *Procedia Eng.*, vol. 168, pp. 351–354, 2016.
- [25] P.-G. Su, J.-H. Yu, I.-C. Chen, H.-C. Syu, S.-W. Chiu, and T.-I. Chou, "Detection of ppb-level NO₂ gas using a portable gas-sensing system with a Fe₂O₃/MWCNTs/WO₃ sensor using a pulsed-UV-LED," *Anal. Methods*, 2019.
- [26] F. Deng, W. Chen, J. Wang, and Z. Wei, "Fabrication of a sensor array based on quartz crystal microbalance and the application in egg shelf life evaluation," *Sensors Actuators, B Chem.*, vol. 265, pp. 394–402, 2018.
- [27] J. Burgués and S. Marco, "Multivariate estimation of the limit of detection by orthogonal partial least squares in temperature-modulated MOX sensors," *Anal. Chim. Acta*, vol. 1019, pp. 49–64, 2018.
- [28] B. Szulczyński, J. Namieśnik, and J. Gębicki, "Determination of Odour Interactions of Three-Component Gas Mixtures Using an Electronic Nose," *Sensors*, vol. 17, no. 10, p. 2380, 2017.
- [29] J. Burgués and S. Marco, "Low power operation of temperature-modulated metal oxide semiconductor gas sensors," *Sensors (Switzerland)*, vol. 18, no. 2, 2018.
- [30] F. Li *et al.*, "Selective Sensing of Gas Mixture via a Temperature Modulation Approach: New Strategy for Potentiometric Gas Sensor Obtaining Satisfactory Discriminating Features," *Sensors*, vol. 17, no. 3, p. 573, Mar. 2017.
- [31] L. Wozniak, P. Kalinowski, G. Jasinski, and P. Jasinski, "FFT analysis of temperature modulated semiconductor gas sensor response for the prediction of ammonia concentration under humidity interference," *Microelectron. Reliab.*, vol. 84, no. April, pp. 163–169, 2018.
- [32] A. Ghosh, A. Maity, R. Banerjee, and S. B. Majumder, "Volatile

- organic compound sensing using copper oxide thin films: Addressing the cross sensitivity issue,” *J. Alloys Compd.*, vol. 692, pp. 108–118, 2017.
- [33] T. Saidi *et al.*, “Ability of discrimination of breath from smoker and non-smoker volunteers by using an electronic nose based on WO₃ nanowires and SnO₂ sensors,” *ISOEN 2017 - ISOCS/IEEE Int. Symp. Olfaction Electron. Nose, Proc.*, pp. 2–4, 2017.
- [34] E. Navarrete, C. Bittencourt, P. Umek, and E. Llobet, “AACVD and gas sensing properties of nickel oxide nanoparticle decorated tungsten oxide nanowires,” *J. Mater. Chem. C*, vol. 6, no. 19, pp. 5181–5192, May 2018.
- [35] W. P. Sari, C. Blackman, Y. Zhu, and J. A. Covington, “AACVD Grown WO₃ Nanoneedles Decorated With Ag/Ag₂O Nanoparticles for Oxygen Measurement in a Humid Environment,” *IEEE Sens. J.*, vol. 19, no. 3, pp. 826–832, 2019.
- [36] T. Saidi *et al.*, “Exhaled breath gas sensing using pristine and functionalized WO₃ nanowire sensors enhanced by UV-light irradiation,” 2018.
- [37] T. Vilic and E. Llobet, “Nickel Doped WO₃ Nanoneedles Deposited by a Single Step AACVD for Gas Sensing Applications,” *Procedia Eng.*, vol. 168, pp. 206–210, 2016.
- [38] E. E. A. Technical, *Air quality in Europe — 2018 report*, no. 12. Luxembourg: European Environment Agency, 2018.
- [39] Sensor Electronic Technology, Inc., “UVTOP320”, <http://www.sensor-ic.com>.
- [40] J. Qi *et al.*, “Application of 3D hierarchical monoclinic-type structural Sb-doped WO₃ towards NO₂ gas detection at low temperature,” *Nanoscale*, vol. 10, no. 16, pp. 7440–7450, 2018.
- [41] C. Zhang, A. Boudiba, C. Bittencourt, R. Snyders, M.-G. Olivier, and M. Debliquy, “Visible light activated tungsten oxide sensors for NO₂ detection at room temperature,” *Procedia Eng.*, vol. 47, pp. 116–119, 2012.
- [42] P. Jaroenapibal, P. Boonma, N. Saksilaporn, M. Horprathum, V. Amornkitbamrung, and N. Triroj, “Improved NO₂ sensing performance of electrospun WO₃ nanofibers with silver doping,” *Sensors Actuators B*, vol. 255, pp. 1831–1840, 2018.